What Are the Sources of Mechanical Damping in Matsuno–Gill-Type Models?

JIA-LIN LIN*

NOAA/ESRL/CIRES Climate Diagnostics Center, Boulder, Colorado

BRIAN E. MAPES

RSMAS, University of Miami, Miami, Florida

WEIQING HAN

DAOS, University of Colorado, Boulder, Colorado

(Manuscript received 19 June 2006, in final form 17 May 2007)

ABSTRACT

The Matsuno–Gill model has been widely used to study the tropical large-scale circulations and atmosphere–ocean interactions. However, a common critique of this model is that it requires a strong equivalent linear mechanical damping to get realistic wind response and it is unclear what could provide such a strong damping above the boundary layer. This study evaluates the sources and strength of equivalent linear mechanical damping in the Walker circulation by calculating the zonal momentum budget using 15 yr (1979–93) of daily global reanalysis data. Two different reanalyses [NCEP–NCAR and 15-yr ECMWF Re-Analysis (ERA-15)] give qualitatively similar results for all major terms, including the budget residual, whose structure is consistent with its interpretation as eddy momentum flux convergence by convective momentum transport (CMT).

The Walker circulation is characterized by two distinct regions: a deep convection region over the Indo-Pacific warm pool and a shallow convection region over the eastern Pacific cold tongue. These two regions are separated by a strong upper-tropospheric ridge and a strong lower-tropospheric trough in the central Pacific. The resultant pressure gradient forces on both sides require strong (approximately 5–10 days) damping to balance them because Coriolis force near the equator is too small to provide the balance. In the deep convection region, the damping is provided by CMT and advection together in both the upper and lower troposphere. In the shallow convection region, on the other hand, the damping is provided mainly by advection in the upper troposphere and by CMT in the lower troposphere. In other words, the upper-level tropical easterly jet and the low-level trade wind are both braked by CMT. These results support the use of strong damping in the Matsuno–Gill-type models but suggest that the damping rate is spatially inhomogeneous and the CMT-related damping increases with the strength of convection. Implications for GCM's simulation of tropical mean climate are discussed.

1. Introduction

A widely used model for tropical large-scale circulations is the linear, dissipative model developed by Matsuno (1966) and revived by Gill (1980). The momentum equation of this model is simply linearized about a state at rest:

$$\frac{\partial \mathbf{V}}{\partial t} = -\nabla\varphi - f\mathbf{k} \times \mathbf{V} - \varepsilon\mathbf{V}, \tag{1}$$

where $\mathbf{V}$ is the wind, φ is the geopotential, f is the Coriolis parameter, and ε is the linear damping coefficient; x and y are east–west and north–south distance. There are three acceleration terms: the pressure gradient force, the Coriolis force, and a linear damping. Amazingly, this simple model can reproduce quite well the basic features of the Walker circulation when using symmetric heating about the equator and a qualitatively monsoonlike circulation when using the linear sum of symmetric and asymmetric heatings (e.g., Gill

* Current affiliation: Department of Geography, The Ohio State University, Columbus, Ohio.

Corresponding author address: Dr. Jia-Lin Lin, Department of Geography, The Ohio State University, Columbus, OH 43210.
E-mail: lin.789@osu.edu

DOI: 10.1175/2007JCLI1546.1

1980; Lau and Lim 1982; Silva Dias et al. 1983; DeMaria 1985; Zhang and Krishnamurti 1996). It has been combined with convective parameterization to simulate the atmospheric response to ENSO (e.g., Zebiak 1982; Seager 1991; Kleeman 1991) and has been frequently used to obtain the low-level atmospheric flow in simple coupled ocean–atmosphere models (e.g., Philander et al. 1984; Gill 1985; Anderson and McCreary 1985; Zebiak and Cane 1987; Schopf and Suarez 1988; Battisti 1988; Battisti and Hirst 1989; Wakata and Sarachik 1991).

Despite the overall success of the Matsuno–Gill model, a common critique of this model is that it requires a rapid damping time scale [on the order of a few days, e.g., 1 day in Gill (1980)] to get realistic wind responses, and it is unclear what could provide such a strong damping above the boundary layer, especially in the upper troposphere (see discussions by Battisti et al. 1999).

If we look at the large-scale momentum equation [cf. Eq. (2) below], there are two terms beside the pressure gradient force and Coriolis force: one is the advective tendency and the other is the eddy momentum flux convergence (EMFC). These two terms are possible sources of the equivalent linear damping. EMFC represents accelerations due to all subgrid-scale processes. Over open ocean, above the boundary layer, it is dominated by convective momentum transport (CMT; also called "cumulus friction" in some of the previous studies). Each of the terms in Eq. (2), except EMFC, can be estimated from analyzed wind and pressure fields, and EMFC can be estimated from the residual of the budget. In this way, we can determine the contributions of the two possible damping terms to the momentum budget.

Several previous studies analyzed the momentum budget of tropical large-scale circulations both at the surface (e.g., Deser 1993; Wang and Li 1993; Chiang and Zebiak 2000) and in the free troposphere (Stevens 1979; Carr and Bretherton 2001; Tung and Yanai 2002a,b; Lin et al. 2005; Dima et al. 2005). Deser (1993) evaluated the surface momentum budget over the tropical Pacific Ocean using the Comprehensive Ocean–Atmosphere Data Set (COADS), derived the friction as a budget residual, and estimated the corresponding linear damping time scales. Stevens (1979) calculated the momentum budget for the Global Atmospheric Research Program (GARP) Atlantic Tropical Experiment (GATE) sounding array in the tropical Atlantic Ocean and found that CMT is as large as other acceleration terms in the synoptic-scale waves. Tung and Yanai (2002a) studied the momentum budget for the Tropical Ocean and Global Atmosphere Coupled Ocean–Atmosphere Response Experiment (TOGA COARE) sounding array in the western Pacific and found that CMT contributes significantly to the Madden–Julian oscillation (MJO) and 2-day waves.

Carr and Bretherton (2001) analyzed the momentum budget using TOGA COARE sounding array data as well as the National Centers for Environmental Prediction (NCEP) and European Centre for Medium-Range Weather Forecasts (ECMWF) reanalysis data during the TOGA COARE 4-month period (November 1992–February 1993). The regions studied include not only the western Pacific but also the central Pacific and eastern Pacific. They found that budget residual is significant at 850 mb in all three regions. Since the subcloud turbulent layer typically does not extend above 940 mb, this suggests an important role of CMT by shallow convection. Another important conclusion of the Carr and Bretherton study is that uncertainties in budget results can be significantly reduced if they are averaged over a large domain and over a long time period.

Recently, Lin et al. (2005) examined the zonal momentum budget of the MJO over the equatorial western Pacific region using 15 yr of daily NCEP and ECMWF reanalysis data. They found that the MJO is a highly viscous oscillation, with a 3–5-day equivalent linear damping time scale in the upper as well as lower troposphere. Upper-level damping is mainly in the form of large-scale advection terms, which are linear in MJO amplitude but involve horizontal and vertical background flow. Specifically, the leading terms are the advection of time-mean zonal shear by MJO vertical motion anomalies and advection of MJO wind anomalies by time-mean ascent. The strong upper-level damping necessitates upper-level geopotential height gradients to maintain the observed zonal wind anomalies over the time scales implied by the MJO's low frequency. The existence of the background flow thus tends to shift MJO temperature perturbations westward so that the warm anomaly ahead (east) of the convective center is shifted back into the convection. This shifting effect is fully realized only for anomalies with a period much longer than the 3–5-day damping time and thus favors the amplification of the MJO more than other higher-frequency modes.

In this study, we extend the Carr and Bretherton (2001) and Lin et al. (2005) studies from selected regions to the whole tropics. The purpose is to evaluate the sources and strength of mechanical damping in the Walker circulation. The issues we address are the following:

1) Is there a strong damping in the Walker circulation? That is, is the use of strong damping in the Matsuno–Gill-type models supported by observation?
2) If there is a strong damping, what are the sources?

The datasets used in this study and the procedure for calculating zonal momentum budget are described in section 2. The quality of momentum budgets is evaluated in section 3 by looking at the general features of budget residuals. The zonal momentum budget result of the Walker circulation is reported in section 4. Summary and discussions are given in section 5.

2. Data and method

The datasets used include 15 yr (1979–99) of daily reanalyses data from two different centers: NCEP (Kalnay et al. 1996) and ECMWF [the 15-yr ECMWF Re-Analysis (ERA-15); Gibson et al. 1997]. The variables used include upper air wind, geopotential height, and vertical pressure velocity on pressure surfaces. The horizontal resolution is 2.5° longitude by 2.5° latitude. The zonal momentum budget is calculated for both reanalyses following Carr and Bretherton (2001), based on the large-scale momentum equation

$$\frac{\partial u}{\partial t} = -\frac{\partial \varphi}{\partial x} + fv - \left(u\frac{\partial u}{\partial x} + v\frac{\partial u}{\partial y} + \omega\frac{\partial u}{\partial p} \right) + X. \quad (2)$$

Here X represents accelerations due to all subgrid-scale processes. Each budget term except X was calculated using daily average data at each 2.5° grid point. The term X is computed as the residual, meaning that all errors in the other terms are included in its observational estimate, requiring caution in interpretation. Derivatives were evaluated using three-point central differencing. The results were then averaged to pentad mean along the equator (between 5°N and 5°S) with a zonal resolution of 10° longitude.

As discussed by Carr and Bretherton (2001), in the free troposphere (above the effects of boundary layer turbulent eddies), over the open ocean (away from the effects of topographically induced gravity waves), it is reasonable to assume that CMT is the dominant subgrid-scale process responsible for the vertical transport of momentum. Under this assumption, we can write

$$X = -\frac{\partial}{\partial p}\overline{u'\omega'}. \quad (3)$$

Here the overbar indicates environmental quantities and primes are perturbations from environmental values. In this way, we define X to be the acceleration of the zonal flow due to the convergence of zonal momentum flux.

In addition to the unresolved accelerations due to CMT, the residuals also contain contributions from gravity waves when the region of interest is close to prominent topography, *surface wind stress, which is usually not considered to be a "convective transport,"* and other possible errors, including 1) poor data coverage over certain geographical regions; 2) errors in the pressure fields (which may be due to errors in measured surface pressure or in hydrostatic calculations of layer thickness); 3) effects of data assimilation, which may introduce some artificial mechanical damping; and 4) various numerical artifacts due to topography, spatial interpolation (the NCEP reanalysis was performed on sigma levels with a spectral advection algorithm and subsequently transformed to the gridded pressure level data we used, making it impossible to maintain complete consistency between our numerical approach and that used in the reanalysis itself), and temporal interpolation (the use of time-averaged data omit the momentum transport by any circulation with a time scale shorter than a day). However, as shown by Carr and Bretherton (2001), in spatial averaging over many grid points, many of the above errors are reduced. A simple consistency check on the residual calculation is to assume that upward momentum fluxes at the tropopause are typically much smaller than their corresponding surface values. Carr and Bretherton (2001) have conducted such a consistency check for both NCEP and ECMWF reanalyses and found that vertical integration of X is consistent with surface zonal wind stress. Therefore they conclude that the budget residual is useful when averaged over a large domain and without a nearby prominent topography. In the present study we do not repeat this consistency check, but will present further evidence in section 3 that the general features of budget residual is consistent with their interpretation as eddy momentum flux convergence by CMT.

To study the convective activity, we also used 15 yr (1979–93) of pentad Climate Prediction Center (CPC) Merged Analysis of Precipitation (CMAP) data (Xie and Arkin 1997) and 8 yr (1986–93) of 3-hourly International Satellite Cloud Climatology Project (ISCCP) D1 cloud data (Rossow and Schiffer 1999). Both datasets were averaged to pentad mean along the equator (between 5°N and 5°S) with a zonal resolution of 10° longitude.

3. General features of the budget residuals

Before analyzing the scientific content of the budget results, the first question is how good the NCEP and ECMWF reanalyses are in terms of the momentum budget. One way to evaluate this is to look at the budget residuals. Do they really represent the effect of CMT, or are they just some noises from data errors?

Parametrically, the effect of CMT on zonal momentum, or cumulus friction, can be expressed as (e.g.,

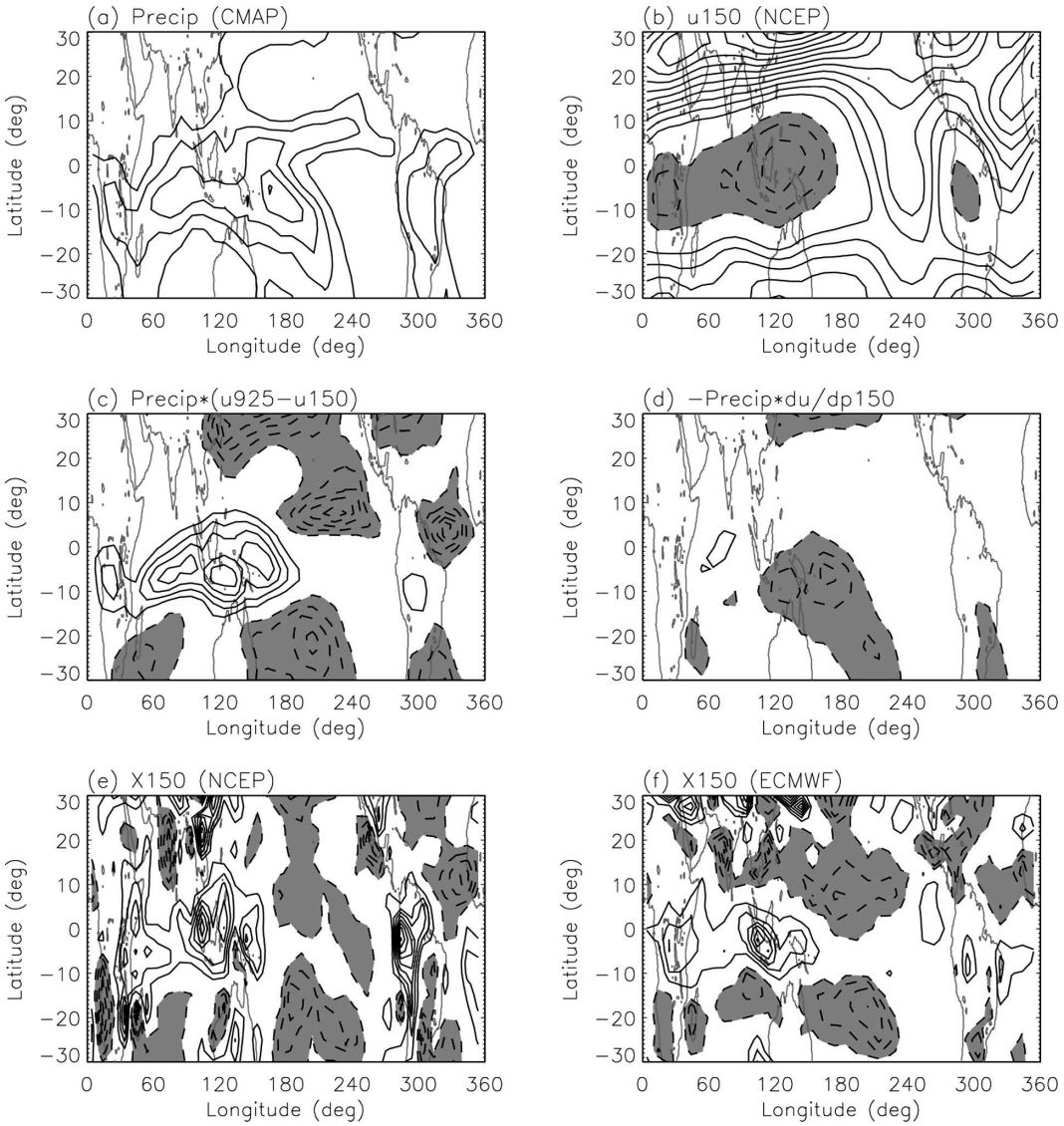

FIG. 1. The 15-yr DJF mean horizontal field of (a) CMAP precipitation (mm day^{-1}), (b) NCEP 150-mb zonal wind (m s^{-1}), (c) precipitation $\times$ ($u_{925\text{mb}} - u_{150\text{mb}}$) (mm day^{-1} $\times$ m s^{-1}), (d) $-$precipitation $\times$ $(\partial u/\partial p)_{150\text{mb}}$ (mm day^{-1} $\times$ m s^{-1} mb^{-1}), (e) NCEP 150-mb X (m s^{-1} day^{-1}), and (f) ECMWF 150-mb X (m s^{-1} day^{-1}). The first contour in (a)–(f) is 3, 5, 40, 0.4, 1.2, and 0.8, respectively. Contour interval is the same as the first contour.

Schneider and Lindzen 1976; Zhang and Cho 1991a; Gregory et al. 1997; Carr and Bretherton 2001):

$$X = -\frac{\partial}{\partial p}\overline{u'\omega'} = -\frac{\partial}{\partial p}[M_c(u_c - u)]$$

$$= \delta_c(u_c - u) - M_c\frac{\partial(u_c - u)}{\partial p}$$

$$= \delta_c(u_b - u) + M_c\frac{\partial u}{\partial p} + \left[\delta_c(u_c - u_b) - M_c\frac{\partial u_c}{\partial p}\right]. \quad (4)$$

Here M_c is the convective mass flux, δ_c is cloud detrainment rate, u_c is in-cloud zonal wind, and u_b is zonal wind at cloud base. The first term represents the effect of wind shear between cloud base and the level of interest. The second term represents the effect of local wind shear. The third term represents the effects of change in in-cloud zonal wind caused by entrainment and across-cloud pressure gradients. Schneider and Lindzen (1976) estimated that the first term is generally much larger than the other two terms. Here we approximate cloud-base u by the value at 925 mb, while both δ_c and M_c are approximately linearly related to precipita-

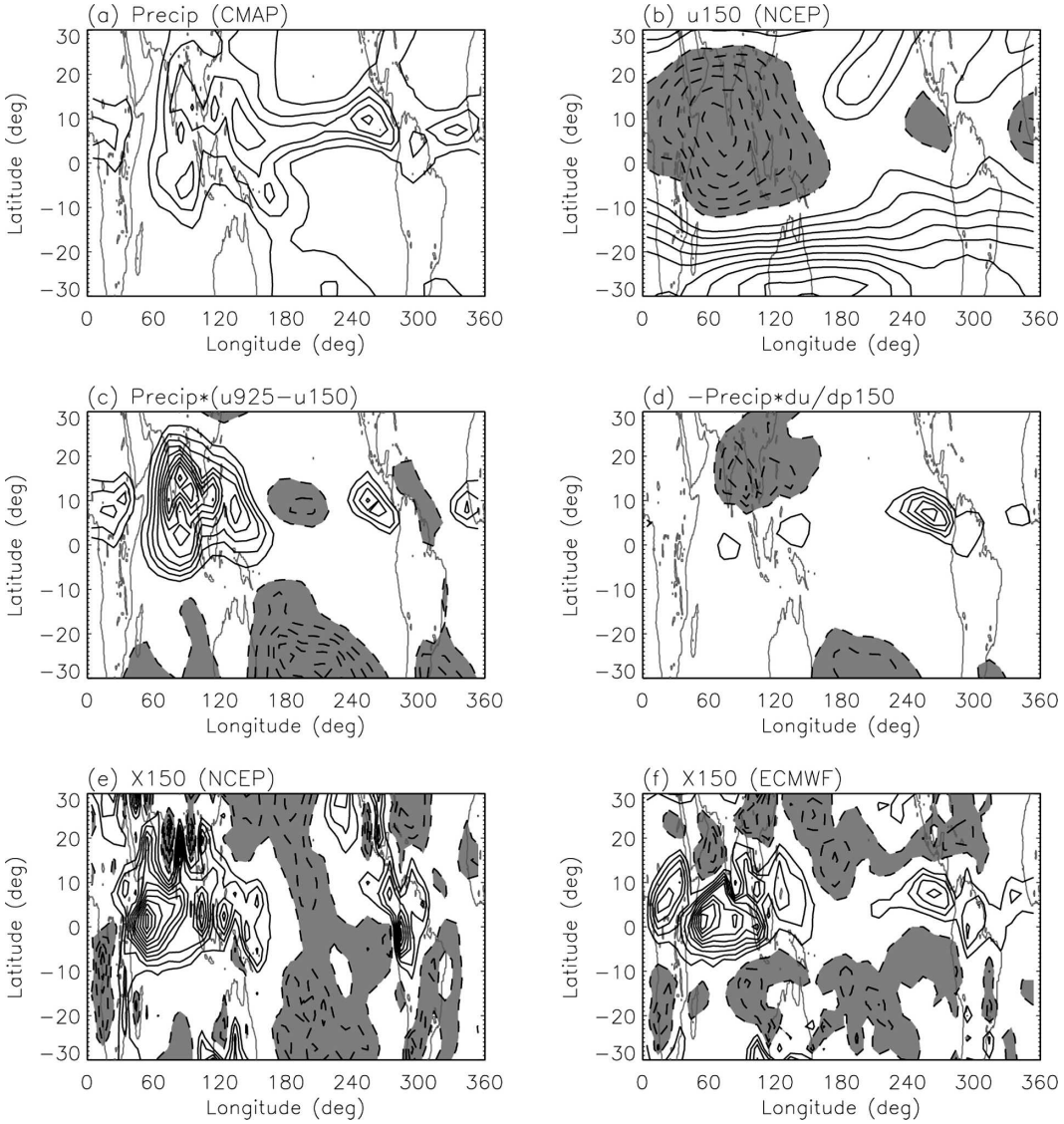

FIG. 2. Same as in Fig. 1 but for JJA.

tion. Figures 1a–f show the 15-yr (1979–93) December–February (DJF) mean horizontal field of CMAP precipitation; NCEP 150-mb zonal wind; precipitation $\times$ $(u_{925\text{mb}} - u_{150\text{mb}})$, which corresponds to the first term in Eq. (4); precipitation $\times$ $(\partial u/\partial p)_{150\text{mb}}$, which corresponds to the second term in Eq. (4); NCEP 150-mb X; and ECMWF 150-mb X. In the northern winter, the precipitation (Fig. 1a) centers slightly south of the equator. This region of the strongest convection also corresponds to the strongest vertical wind shear because of the upper-level tropical easterly jet (Fig. 1b). The product between precipitation and deep wind shear, precipitation $\times$ $(u_{925\text{mb}} - u_{150\text{mb}})$, (Fig. 1c) shows large positive values over the region of tropical easterly jet and strong precipitation and large negative values over the regions with upper-level westerly wind and strong precipitation. The product between precipitation and local wind shear, precipitation $\times$ $(\partial u/\partial p)_{150\text{mb}}$, (Fig. 1d) shows negative values over the South Pacific convergence zone (SPCZ) and subtropical north Pacific. Over the open oceans, the budget residual from NCEP reanalysis (Fig. 1e) displays a pattern quite similar to that of precipitation $\times$ $(u_{925\text{mb}} - u_{150\text{mb}})$ (Fig. 1c), suggesting that it does represent the effect of cumulus friction. Large values of X are also seen near the prominent topography (e.g., South America and East Africa), which may be caused by gravity waves or numerical artifacts related to topography. The ECMWF reanalysis (Fig. 1f) shows a similar feature but with a weaker magnitude, which is likely caused by differences be-

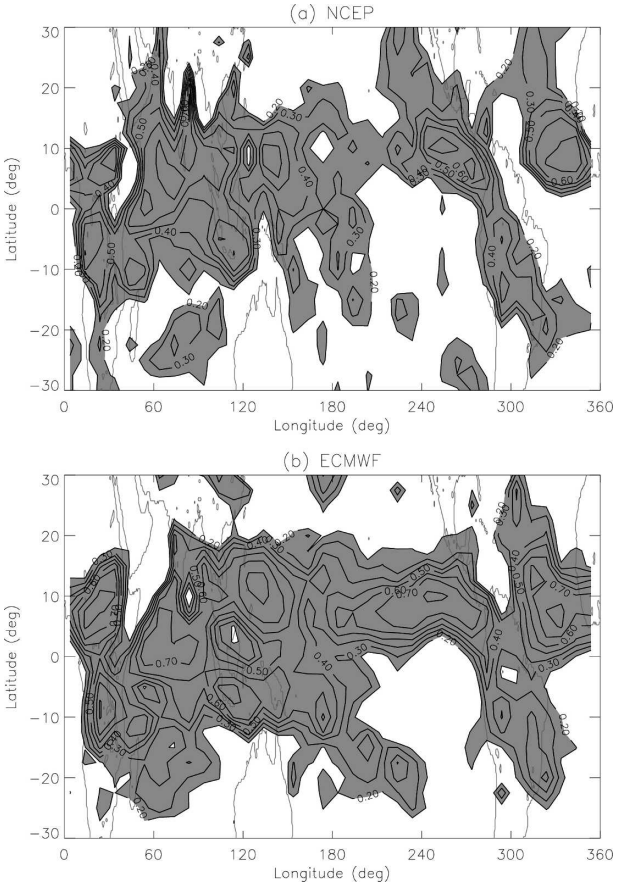

FIG. 3. Correlation coefficient between monthly-mean 150-mb X and precipitation $\times$ ($u_{925\text{mb}} - u_{150\text{mb}}$) for (a) NCEP and (b) ECMWF data. The 99% confidence level is 0.2. The first contour is 0.2 and the contour interval is 0.1.

tween the two assimilation systems (e.g., in analysis method, model dynamics, and model physics).

Figure 2 is the same as in Fig. 1 but for the northern summer. The center of the strongest convection moves to the north of the equator (Fig. 2a), together with the tropical easterly jet (Fig. 2b). Consistently, precipitation $\times$ ($u_{925\text{mb}} - u_{150\text{mb}}$) (Fig. 2c) shows large positive values over the Asian monsoon region and large negative values over SPCZ and subtropical southern Indian Ocean. Precipitation $\times$ $(\partial u/\partial p)_{150\text{mb}}$ (Fig. 2d) shows negative values over the Asian monsoon region and SPCZ. The budget residual (Figs. 2e,f) again has a similar pattern as precipitation $\times$ ($u_{925\text{mb}} - u_{150\text{mb}}$) (Fig. 2c). Therefore, the budget residual correlates well in space with the product between precipitation and deep wind shear.

Next we look at the temporal correlation. Figures 3a and 3b show the map of correlation coefficient between the budget residual X and precipitation $\times$ ($u_{925\text{mb}} - u_{150\text{mb}}$) for NCEP and ECMWF data. The correlation coefficient is generally larger than the 99% confidence level over the deep convection regions between 10°N and 10°S. Therefore, the budget residual correlates well both in time and space with precipitation $\times$ ($u_{925\text{mb}} - u_{150\text{mb}}$), which is consistent with its interpretation as eddy momentum flux convergence by CMT. This corroborates the results of Carr and Bretherton (2001).

4. Zonal momentum budget of the Walker circulation

Figures 4a–d show the longitude–height section of annual mean ISCCP cloud fraction, NCEP vertical motion, NCEP zonal wind, and NCEP geopotential height along the equator averaged between 5°N and 5°S. Zonal mean has been removed for geopotential height. Negative values are light shaded, and continents are dark shaded. As shown by Fig. 4a, the Walker circulation is characterized by two distinct regions: a deep convection region over the Indo-Pacific warm pool and a shallow convection region over the eastern Pacific cold tongue. The large-scale vertical motion (Fig. 4b) is upward in the deep convection region but downward in the shallow convection region. In the deep convection region, the zonal wind is characterized by strong easterly (tropical easterly jet) in the upper troposphere and weak westerly in the lower troposphere, while in the shallow convection region, it is characterized by strong westerly in the upper troposphere and strong easterly trade wind in the lower troposphere (Fig. 4c). Most important to this study, the deep and shallow convection regions are separated by a strong upper-tropospheric ridge and a strong lower-tropospheric trough in the central Pacific (Fig. 4d).

Figures 5a–d are the same as in Fig. 4 but for the different components of the zonal momentum budget from NCEP reanalysis, including pressure gradient force, Coriolis force, total advective tendency, and X. The upper-tropospheric ridge in the central Pacific (Fig. 4d) causes strong pressure gradient forces on both sides of it, as is shown in Fig. 5a. There is a westward pressure gradient force over the deep convection region and an eastward pressure gradient force over the shallow convection region.

What balances these strong pressure gradient forces? Near the equator, the Coriolis force is small (Fig. 5b). In the deep convection region, NCEP reanalysis shows that the advection is also small (Fig. 5c), and the pressure gradient force is mainly balanced by the convective momentum flux convergence (Fig. 5d). In the shallow convection region, the strong pressure gradient force is balanced by advection in the upper troposphere (Fig. 5c) and convective momentum flux convergence in the lower troposphere (Fig. 5d).

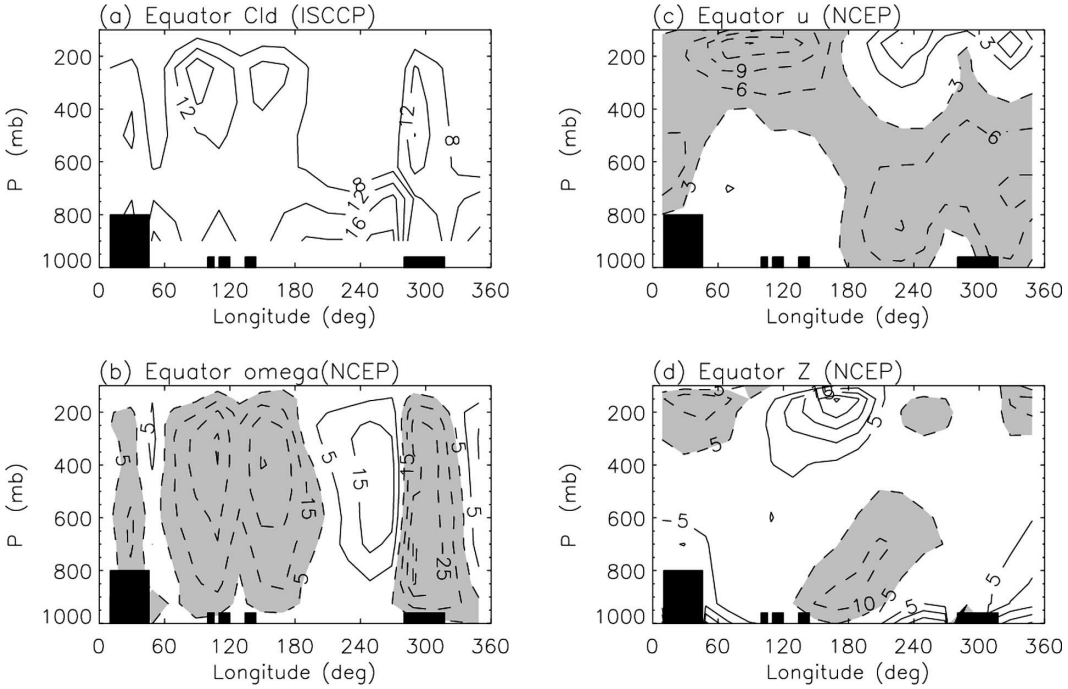

FIG. 4. Annual mean (a) cloud fraction for 8 yr (1986–93) of ISCCP D1 data, and (b) ω (mb day^{-1}), (c) u (m s^{-1}), and (d) Z (m, from which zonal mean is removed) for 15 yr (1979–93) of NCEP reanalysis data along the equator averaged between 5°N and 5°S. Negative values are light shaded. Continents are dark shaded.

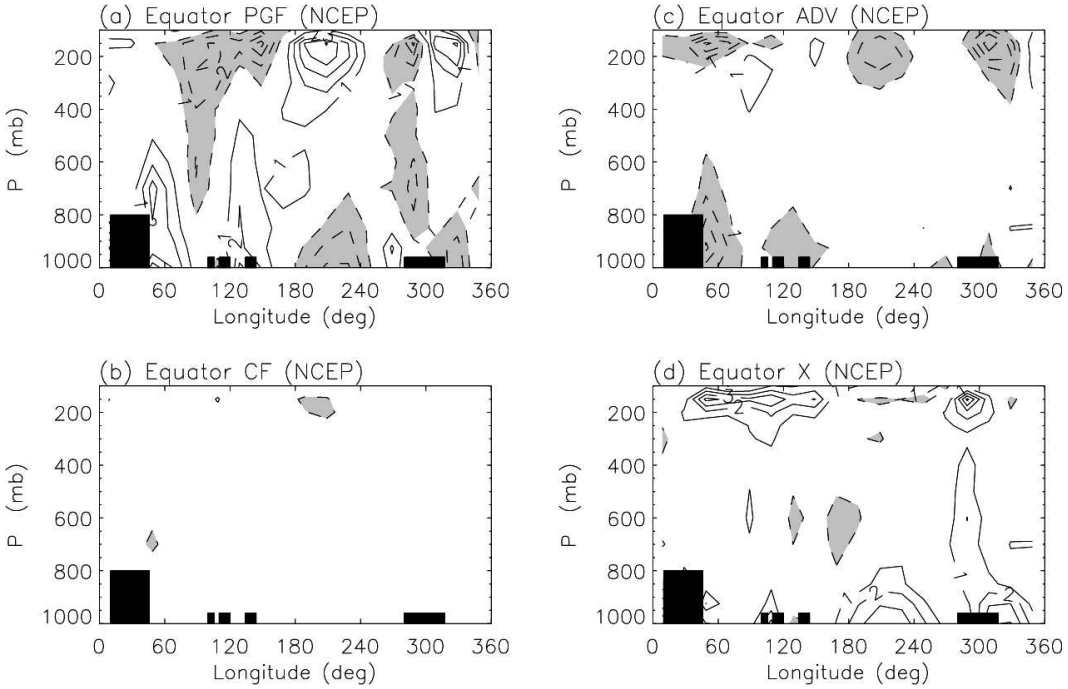

FIG. 5. Same as in Fig. 4 but for (a) pressure gradient force, (b) Coriolis force, (c) total advective tendency, and (d) residual. Unit is m s^{-1} day^{-1}.

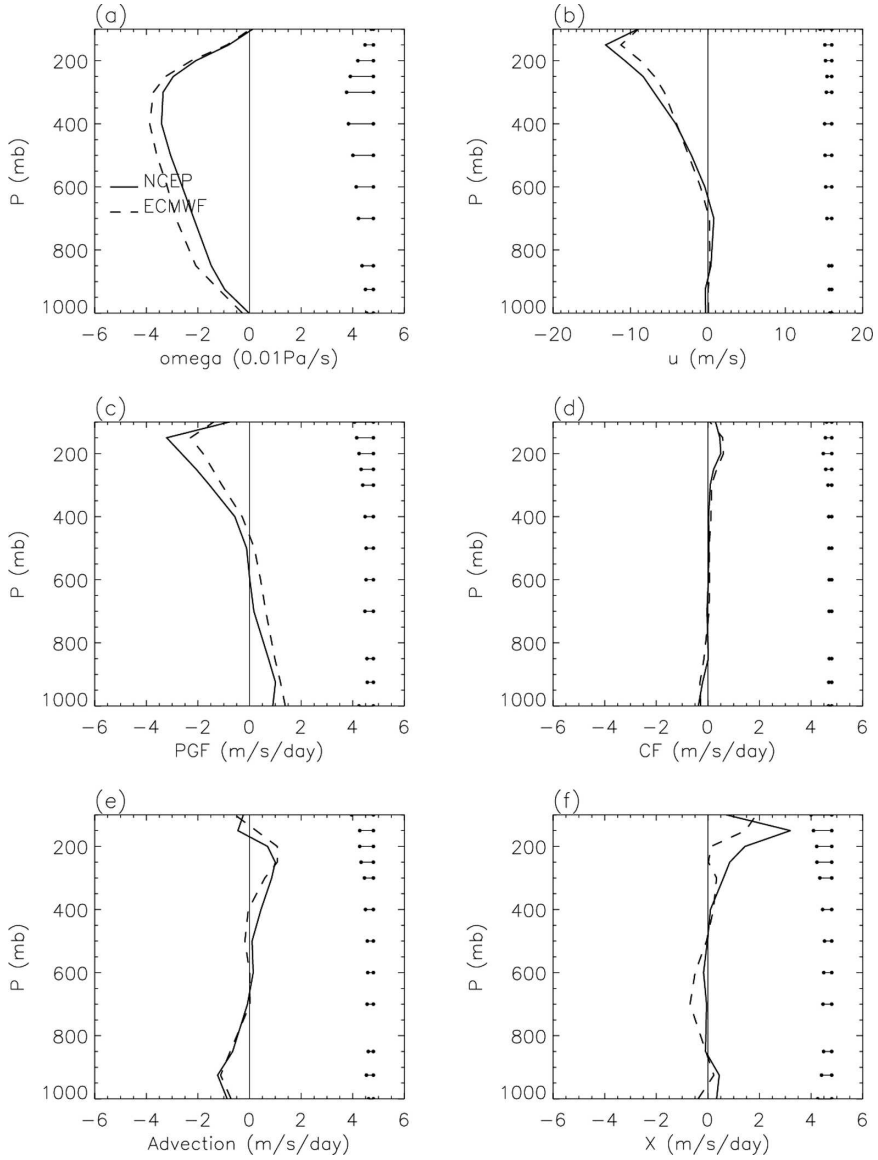

FIG. 6. Vertical profile of annual mean (a) ω, (b) u, (c) pressure gradient force, (d) Coriolis force, (e) advective tendency, and (f) budget residual for 15 yr (1979–93) of NCEP (solid line) and ECMWF (dashed line) reanalyses data averaged over the deep convection region (5°N–5°S and 80°–160°E).

The above results are from the NCEP reanalysis. To give a quantitative comparison between the two reanalyses, following Carr and Bretherton (2001), we average the budget results over large domains, in this case, over the whole deep convection region and the whole shallow convection region. Figure 6 shows the 15-yr-averaged vertical profiles for the deep convection region. The solid line is for NCEP reanalysis and the dashed line is for ECMWF reanalysis. To give an estimate of the error bars for the state variables and budget components, again following Carr and Bretherton (2001), in Fig. 6 we overplot the standard deviation of the differences between the two reanalyses for monthly mean data (the horizontal bars). We can see that the standard deviations are small, suggesting that the two reanalyses are quite consistent with each other. The deep convection region is characterized by climatological mean upward motion with the maximum around 300–400 mb (Fig. 6a) and the strong tropical easterly jet around 150 mb (Fig. 6b). There is a strong pressure gradient force in the upper troposphere (Fig. 6c), which is caused by the strong ridge in the central Pacific (Fig. 4d). The strong pressure gradient force is balanced mainly by the advection below 175 mb (Fig. 6e) and

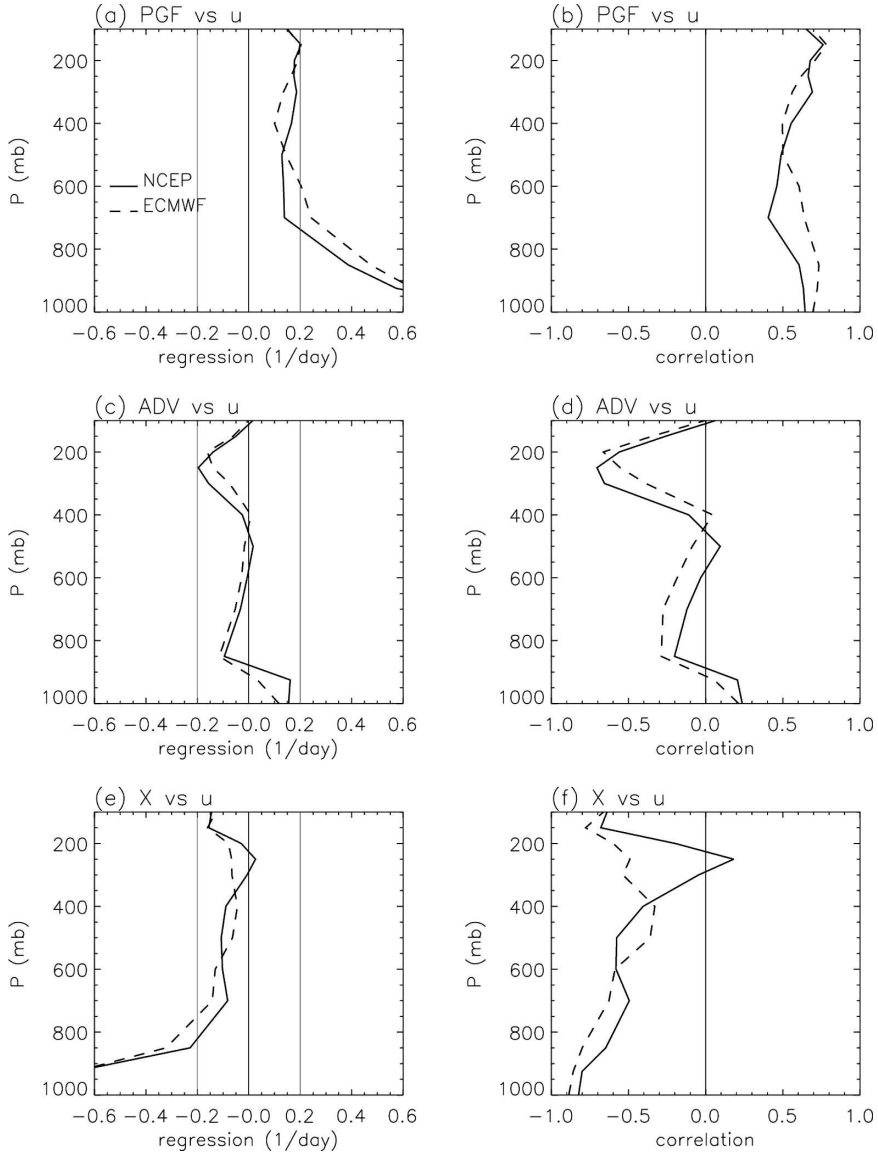

FIG. 7. Vertical profile of linear regression coefficient of the monthly-mean (a) pressure gradient force, (c) advective tendency, and (e) budget residual, with respect to the zonal wind at the same level for 15 yr (1979–93) of NCEP (solid line) and ECMWF (dashed line) reanalyses data averaged over the deep convection region (5°N–5°S and 80°–160°E); (b), (d), (f) the corresponding correlation coefficients.

by the convective momentum flux convergence above 175 mb (Fig. 6f).

How large, then, is the equivalent linear damping rate? A comparison between Eqs. (1) and (2) gives

$$\varepsilon u = \left(u \frac{\partial u}{\partial x} + v \frac{\partial u}{\partial y} + \omega \frac{\partial u}{\partial p} \right) - X.$$

We estimate the equivalent linear damping rate ε by regressing the monthly-mean zonal momentum budget terms onto the monthly-mean zonal wind u. Figure 7 shows the vertical profiles of linear regression coefficients in units of day^{-1}, that is, 0.2 day^{-1} corresponds to a 5-day damping. The pressure gradient force (Fig. 7a) is equivalent to a 5–10-day forcing in the upper troposphere. That is to say, it requires a 5–10-day damping to balance it. This damping is provided by the advection below 175 mb (Fig. 7c) and by the convective momentum flux convergence above 175 mb (Fig. 7e). The correlation coefficients (Figs. 7b,d,f) are generally large whenever regression coefficients are large, suggesting

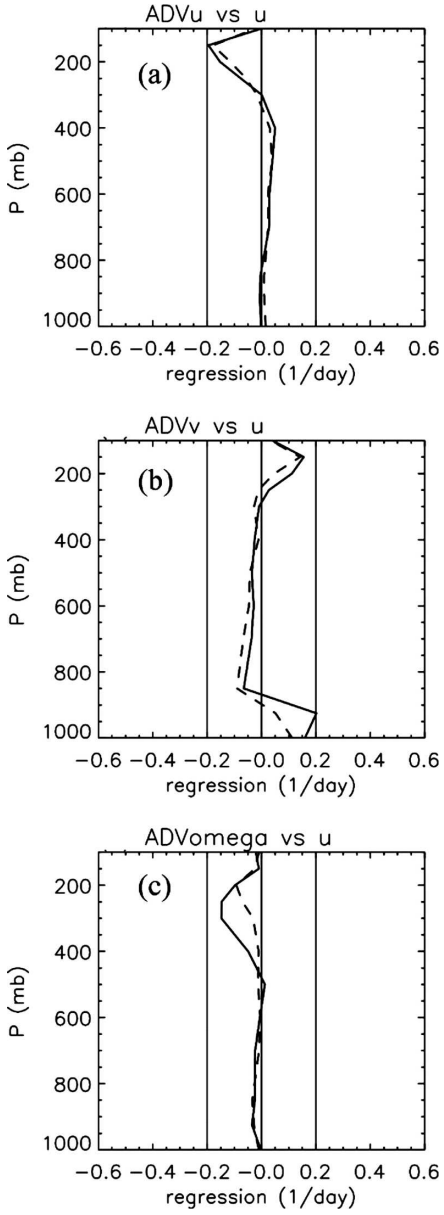

FIG. 8. Same as in Fig. 7 but for (a) zonal, (b) meridional, and (c) vertical components of advective tendency.

that to the first-order approximation, it is appropriate to assume the corresponding mechanical damping terms to be linear.

The advective tendency (Fig. 7c) has three components: zonal, meridional, and vertical advections, which are plotted in Figs. 8a–c, respectively. All three components contribute significantly to the large total advective tendency below 200 mb (Fig. 7c), while the large total advective tendency near the surface is mainly caused by the meridional component (Fig. 8b).

For the shallow convection region (Fig. 9), the two reanalyses both show upward motion in the lower levels and downward motion in the upper levels (Fig. 9a), consistent with the dominance of shallow cloud in this region (Fig. 4a). However, there is significant difference in the detailed shape of the vertical profile and the position of the peaks. This is not surprising because the vertical motion strongly depends on the convective parameterization (both the deep and shallow convection schemes) in the assimilation models. Fortunately, the significant difference in vertical motion between the two reanalyses does not cause much difference in the zonal momentum budget because the vertical advection is much smaller than other budget terms, as will be shown shortly in Fig. 11.

Unlike the vertical motion, the two reanalyses are quite consistent in zonal wind (Fig. 9b) and the zonal momentum budget terms (Figs. 9c–f). There is a strong pressure gradient force in both the upper and lower levels (Fig. 9c), which is caused by the central Pacific upper-level ridge and lower-level trough, respectively (Fig. 4d). In the upper level, the strong pressure gradient force is mainly balanced by advection (Fig. 9e), which agrees with the lack of deep convection in this region (Fig. 4a). In the lower level, the strong pressure gradient force is balanced by the convective momentum flux convergence (Fig. 9f), consistent with the abundance of shallow trade wind clouds in this region (Fig. 4a).

When scaled by the zonal wind, the pressure gradient force is equivalent to a 5-day forcing above 300 mb and a 5-day or larger forcing below 850 mb (Fig. 10a), which means that it requires such a strong damping to balance it. The damping in the upper troposphere is provided by the advective tendency (Fig. 10c), while that in the lower troposphere is provided by the convective momentum flux convergence (Fig. 10e). The correlation coefficients (Figs. 10b,d,f) are generally large whenever regression coefficients are large, suggesting that to the first-order approximation, it is appropriate to assume the corresponding mechanical damping terms to be linear.

The three components of the advective tendency (Fig. 10c) are plotted in Fig. 11. The strong advective tendency in the upper troposphere is contributed by both the zonal (Fig. 11a) and meridional (Fig. 11b) components. The vertical component is quite small in both reanalyses (Fig. 11c). Therefore, although the two reanalyses have substantial difference in vertical motion (Fig. 9a), it does not affect the zonal momentum budget much.

The above zonal momentum budget results are for the vertical cross section along the equator averaged between 5°N and 5°S. It is important to note that the equivalent linear damping rate is actually spatially in-

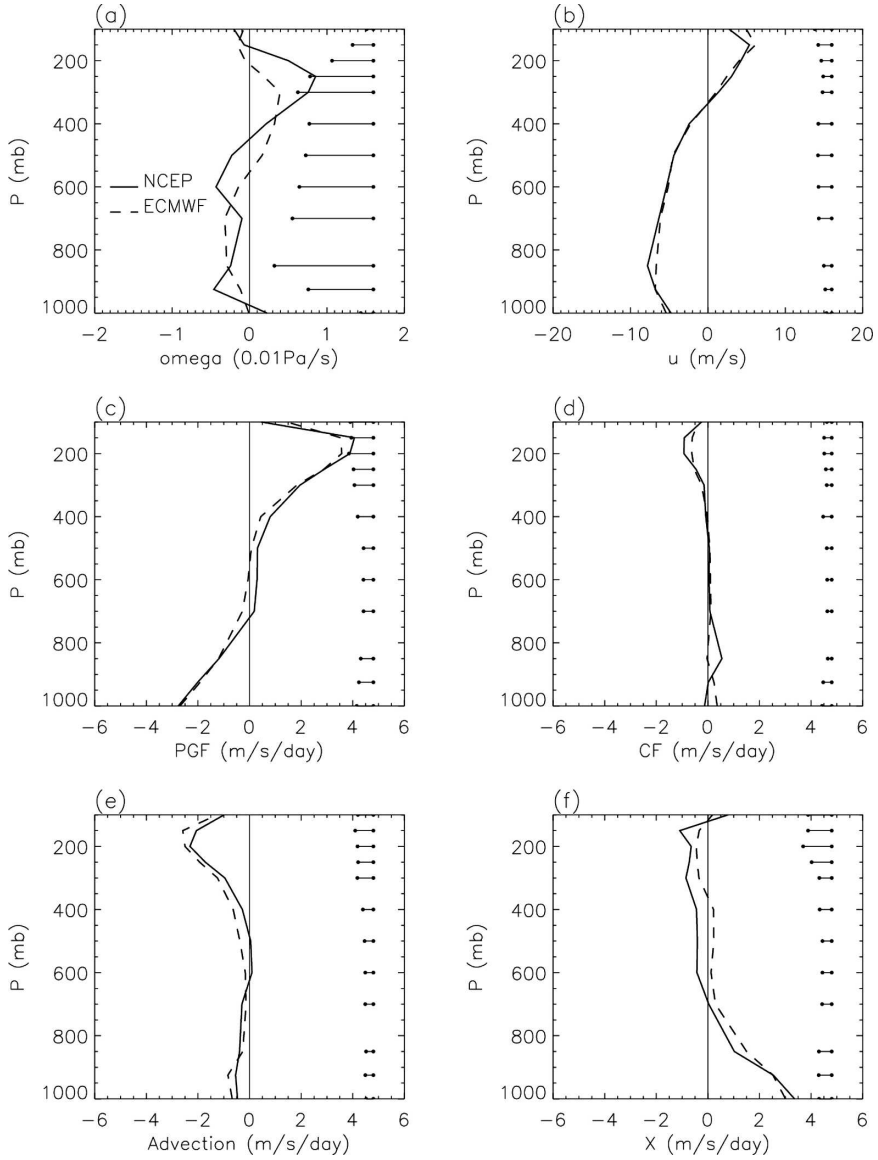

FIG. 9. Same as in Fig. 6 but for the shallow convection region (5°N–5°S, 180°–240°E).

homogeneous. Both Eq. (4) and the results shown in section 3 suggest that the damping rate due to X should increase with the strength of convection. Figures 12a and 12b show the horizontal map of linear regression coefficient between 150-mb X and 150-mb u for NCEP and ECMWF data. Over the open oceans, the regression coefficient is indeed larger in regions with stronger precipitation.

5. Summary and discussions

The Matsuno–Gill model has been widely used to study the tropical large-scale circulations and atmosphere–ocean interactions. However, a common critique of this model is that it requires a strong equivalent linear mechanical damping to get realistic wind response and it is unclear what could provide such a strong damping above the boundary layer. This study evaluates the sources and strength of equivalent linear mechanical damping in the Walker circulation by calculating the zonal momentum budget using 15 yr (1979–93) of daily global reanalysis data. Two different reanalyses [NCEP–National Center for Atmospheric Research (NCAR) and ERA-15] give qualitatively similar results for all major terms, including the budget residual, whose structure is consistent with its interpretation as eddy momentum flux convergence by convective momentum transport.

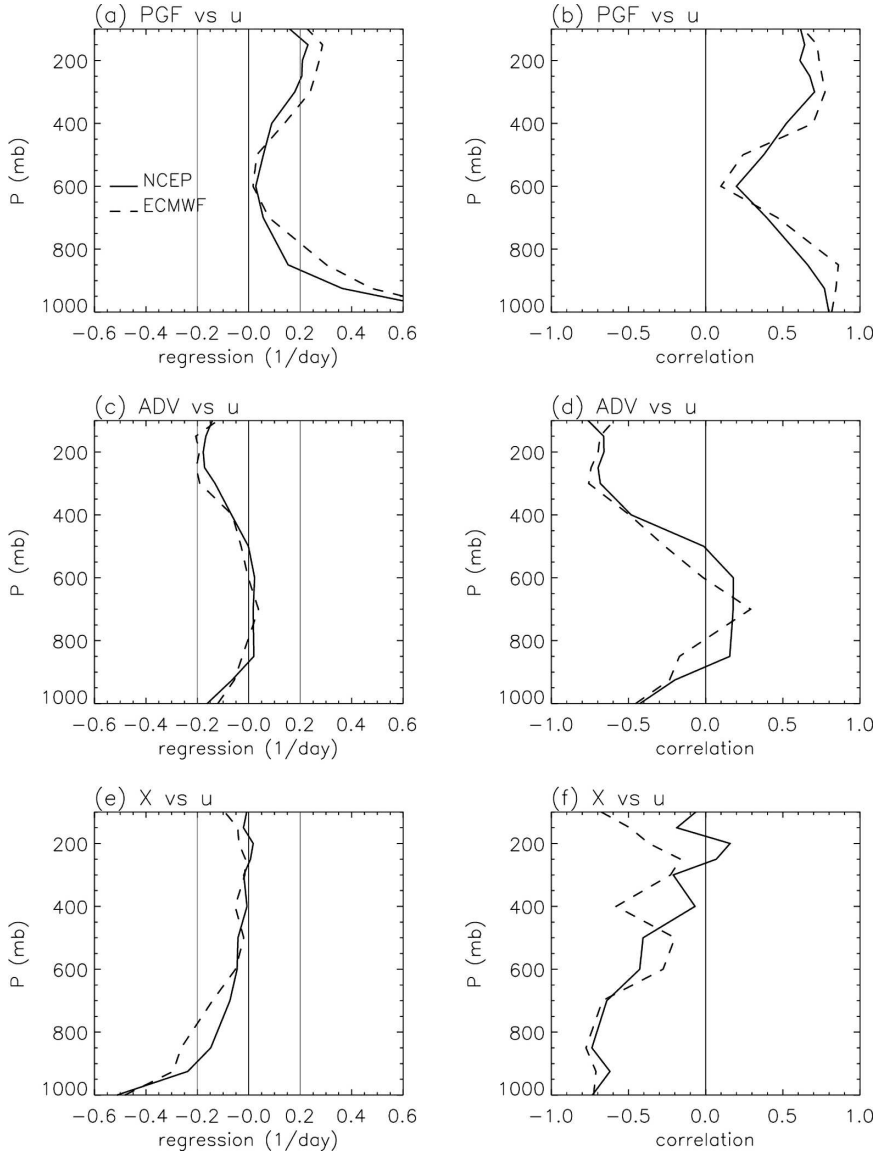

FIG. 10. Same as in Fig. 7 but for the shallow convection region (5°N–5°S, 180°–240°E).

The zonal momentum budget of the Walker circulation is summarized schematically in Fig. 13. The Walker circulation is characterized by two distinct regions, a deep convection region over the Indo-Pacific warm pool and a shallow convection region over the eastern Pacific cold tongue. These two regions are separated by a strong upper-tropospheric ridge and a strong lower-tropospheric trough in central Pacific. The resultant pressure gradient forces on both sides require strong (approximately 5–10 days) damping to balance them because Coriolis force near the equator is too small to provide the balance. In the deep convection region, the damping is provided by CMT and advection together in both the upper and lower troposphere. In the shallow convection region, on the other hand, the damping is provided mainly by advection in the upper troposphere and by CMT in the lower troposphere. In other words, the upper-level tropical easterly jet and the low-level trade wind are both braked by CMT.

The above results support the use of strong damping in the Matsuno–Gill-type models. However, it is important to note that the damping rate suggested by observations is spatially inhomogeneous, which seems to actually be quite a strong function of the heating rate, as prescribed by the deep convective or shallow clouds. It seems that this can easily be incorporated in a moist closure of Matsuno–Gill models.

Our results have important implications for GCM's

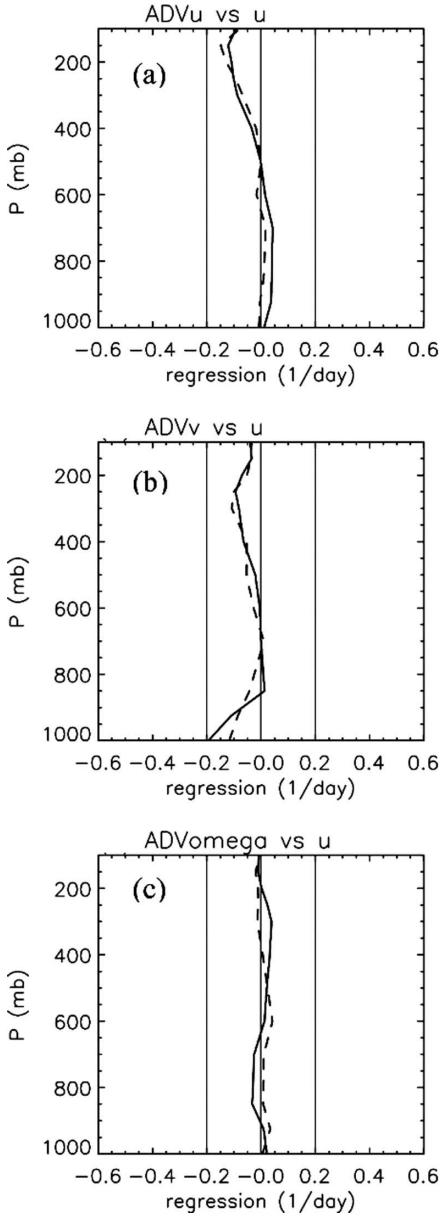

FIG. 11. Same as in Fig. 8 but for the shallow convection region (5°N–5°S, 180°–240°E).

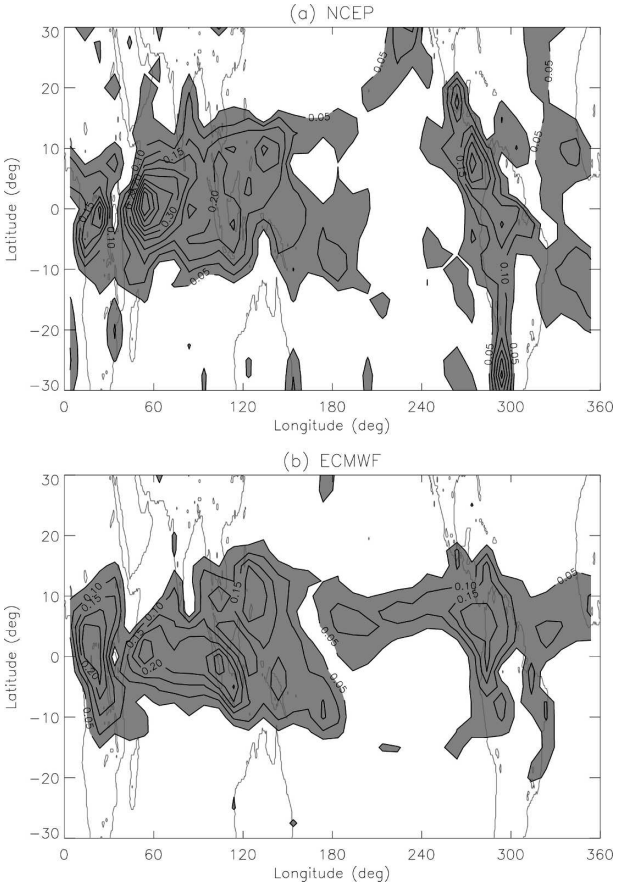

FIG. 12. Linear regression coefficient between monthly 150-mb X and 150-mb u for (a) NCEP and (b) ECMWF data. Only values with correlation coefficient larger than the 99% confidence level are plotted. The first contour is 0.05, and the contour interval is 0.05.

simulation of tropical mean climate. Because the convective momentum flux convergence is a dominant term of zonal momentum balance and brakes both the upper-level tropical easterly jet and the lower-level trade winds, it needs to be considered in the GCMs. However, convective momentum transport has not been included in many GCMs, which makes the form of their zonal momentum balance questionable. GCM experiments have shown that the simulated tropical mean climate is very sensitive to the inclusion of CMT (e.g., Gregory et al. 1997; Inness and Gregory 1997; Wu et al. 2003). Gregory et al. (1997) found that including a CMT parameterization significantly weakens the upper-level tropical easterly jet in the Met Office (UKMO) GCM, which is consistent with our observational results. Wu et al. (2003) found that including a CMT parameterization substantially improves the simulation of the seasonal migration of ITCZ in the NCAR GCM, which is caused by CMT-induced secondary meridional circulation. Another interesting result is that including a CMT parameterization significantly alleviated the double-ITCZ problem (i.e., insufficient precipitation on the equator in the warm pool region but excessive precipitation off the equator) in the Geophysical Fluid Dynamics Laboratory (GFDL) GCM (I. Held 2004, personal communication). This may be understood based on the model of tropical mean climate by Wang and Li (1993), which is a Matsuno–Gill-type model with a frictional boundary layer. They found that when the frictional layer is thin, the

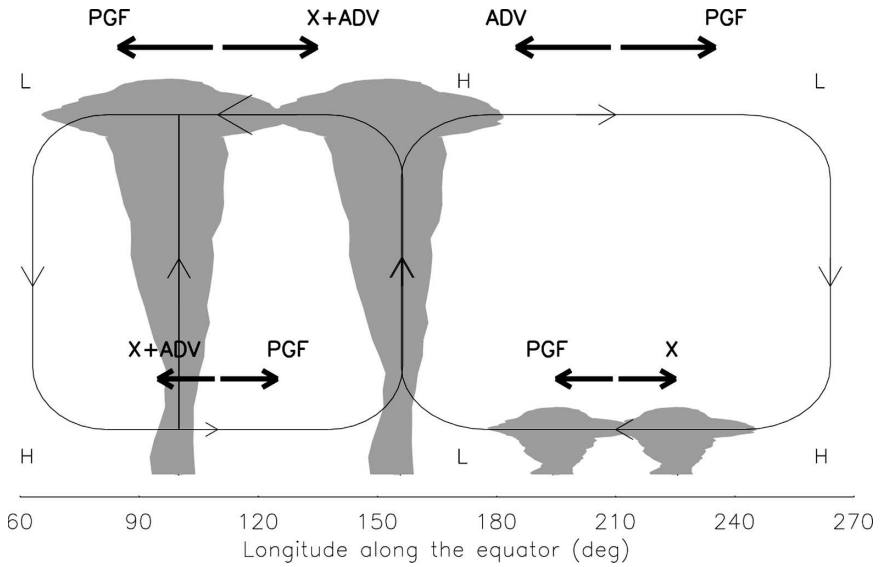

FIG. 13. Schematic depiction of the zonal momentum budget of the Walker circulation. "H" and "L" represent the high and low geopotential heights, respectively. Thin arrows represent the winds. Thick arrows represent the components of the zonal momentum budget.

climatological mean precipitation tends to show a double-ITCZ pattern with maximum precipitation off the equator and little precipitation on the equator, but when the frictional layer is thick, the double-ITCZ pattern disappears and the maximum precipitation concentrates on the equator (see Wang and Li 1993, their Figs. 10a,b). This may be because a thicker frictional layer favors precipitation over the region with the highest low-level moisture (which in turn is the region with the warmest SST right on the equator) through the frictional wave–convective instability of the second kind (CISK) mechanism. As shown in Figs. 7e and 10e, the shallow convective momentum transport causes strong mechanical damping above the boundary layer up to 850 mb, which makes the frictional layer much thicker than the boundary layer (usually with top below 940 mb) and thus may help to alleviate the double-ITCZ problem. Unfortunately, convective momentum transport has not been included in many GCMs. Several schemes have been developed (e.g., Zhang and Cho 1991a,b; Tiedtke 1993; Wu and Yanai 1994; Zhang and McFarlane 1995; Kershaw and Gregory 1997; Zhang and Wu 2003; Zhu and Bretherton 2004), and the results of the current study provide a baseline for evaluating the parameterization of these schemes.

Acknowledgments. This study benefits from discussions with Hua-Lu Pan, Klaus Weickmann, Chris Bretherton, Minghua Zhang, George Kiladis, Clara Deser, Adam Sobel, and Xiaoqing Wu. The careful and insightful reviews of Paul Kushner and three anonymous reviewers helped a lot to improve the manuscript. J. L. Lin was supported by the NOAA CPO/CVP Program, NOAA CPO/CDEP Program, and NASA MAP Program. B. E. Mapes was supported by the NOAA CPO/CVP Program and by CPO/CPPA Grant GC05-039. W. Han was supported by NSF OCE-0452917 and NASA Ocean Vector Winds Program Award 1283568.

REFERENCES

Anderson, D. L. T., and J. P. McCreary, 1985: Slowly propagating disturbances in a coupled ocean-atmosphere model. *J. Atmos. Sci.,* **42,** 615–629.

Battisti, D. S., 1988: Dynamics and thermodynamics of a warming event in a coupled tropical atmosphere–ocean model. *J. Atmos. Sci.,* **45,** 2889–2919.

——, and A. C. Hirst, 1989: Interannual variability in a tropical atmosphere–ocean model: Influence of the basic state, ocean geometry and nonlinearity. *J. Atmos. Sci.,* **46,** 1687–1712.

——, E. S. Sarachik, and A. C. Hirst, 1999: A consistent model for the large-scale steady surface atmospheric circulation in the Tropics. *J. Climate,* **12,** 2956–2964.

Carr, M. T., and C. S. Bretherton, 2001: Convective momentum transport over the tropical Pacific: Budget estimates. *J. Atmos. Sci.,* **58,** 1673–1693.

Chiang, J. C. H., and S. E. Zebiak, 2000: Surface wind over tropical oceans: Diagnosis of the momentum balance, and modeling the linear friction coefficient. *J. Climate,* **13,** 1733–1747.

DeMaria, M., 1985: Linear response of a stratified tropical atmosphere to convective forcing. *J. Atmos. Sci.,* **42,** 1944–1959.

Deser, C., 1993: Diagnosis of the surface momentum balance over the tropical Pacific Ocean. *J. Climate,* **6,** 64–74.

Dima, I. M., J. M. Wallace, and I. Kraucunas, 2005: Tropical zonal momentum balance in the NCEP reanalyses. *J. Atmos. Sci.,* **62,** 2499–2513.

Gibson, J. K., P. Kållberg, S. Uppala, A. Hernandez, A. Nomura, and E. Serrano, 1997: ERA description. ECMWF Reanalysis Project Rep. Series 1, 86 pp.

Gill, A. E., 1980: Some simple solutions for heat-induced tropical circulation. *Quart. J. Roy. Meteor. Soc.,* **106,** 447–462.

——, 1985: Elements of coupled ocean–atmosphere models for the tropics. *Coupled Ocean–Atmosphere Models,* J. Nihoul, Ed., Elsevier Oceanography Series, Vol. 40, Elsevier, 303–327.

Gregory, D., R. Kershaw, and P. M. Inness, 1997: Parametrization of momentum transport by convection. II: Tests in single-column and general circulation models. *Quart. J. Roy. Meteor. Soc.,* **123,** 1153–1183.

Inness, P. M., and D. Gregory, 1997: Aspects of the intraseasonal oscillation simulated by the Hadley Centre atmospheric model. *Climate Dyn.,* **13,** 441–458.

Kalnay, E., and Coauthors, 1996: The NCEP/NCAR 40-Year Reanalysis Project. *Bull. Amer. Meteor. Soc.,* **77,** 437–471.

Kershaw, R., and D. Gregory, 1997: Parametrization of momentum transport by convection. I: Theory and cloud modelling results. *Quart. J. Roy. Meteor. Soc.,* **123,** 1133–1151.

Kleeman, R., 1991: A simple model of the atmospheric response to ENSO sea surface temperature anomalies. *J. Atmos. Sci.,* **48,** 3–18.

Lau, K.-M., and H. Lim, 1982: Thermally driven motions in an equatorial β-plane: Hadley and Walker circulations during the winter monsoon. *Mon. Wea. Rev.,* **110,** 336–353.

Lin, J.-L., M. H. Zhang, and B. Mapes, 2005: Zonal momentum budget of the Madden–Julian oscillation: The source and strength of equivalent linear damping. *J. Atmos. Sci.,* **62,** 2172–2188.

Matsuno, T., 1966: Quasi-geostrophic motions in the equatorial area. *J. Meteor. Soc. Japan,* **44,** 25–43.

Philander, S. G. H., T. Yamagata, and R. C. Pacanowski, 1984: Unstable air–sea interactions in the Tropics. *J. Atmos. Sci.,* **41,** 604–613.

Rossow, W. B., and R. A. Schiffer, 1999: Advances in understanding clouds from ISCCP. *Bull. Amer. Meteor. Soc.,* **80,** 2261–2287.

Schneider, E. K., and R. S. Lindzen, 1976: A discussion of the parameterization of momentum exchange by cumulus convection. *J. Geophys. Res.,* **81,** 3158–3161.

Schopf, P. S., and M. J. Suarez, 1988: Vacillations in a coupled ocean–atmosphere model. *J. Atmos. Sci.,* **45,** 549–566.

Seager, R., 1991: A simple model of the climatology and variability of the low-level wind field in the Tropics. *J. Climate,* **4,** 164–179.

Silva Dias, P. L., W. H. Schubert, and M. DeMaria, 1983: Large-scale response of the tropical atmosphere to transient convection. *J. Atmos. Sci.,* **40,** 2689–2707.

Stevens, D. E., 1979: Vorticity, momentum and divergence budgets of synoptic-scale wave disturbances in the tropical Eastern Atlantic. *Mon. Wea. Rev.,* **107,** 535–550.

Tiedtke, M., 1993: Representation of clouds in large-scale models. *Mon. Wea. Rev.,* **121,** 3040–3061.

Tung, W.-W., and M. Yanai, 2002a: Convective momentum transport observed during the TOGA COARE IOP. Part I: General features. *J. Atmos. Sci.,* **59,** 1857–1871.

——, and ——, 2002b: Convective momentum transport observed during the TOGA COARE IOP. Part II: Case studies. *J. Atmos. Sci.,* **59,** 2535–2549.

Wakata, Y., and E. S. Sarachik, 1991: Unstable coupled atmosphere–ocean basin modes in the presence of a spatially varying basic state. *J. Atmos. Sci.,* **48,** 2060–2077.

Wang, B., and T. Li, 1993: A simple tropical atmosphere model of relevance to short-term climate variations. *J. Atmos. Sci.,* **50,** 260–284.

Wu, X., and M. Yanai, 1994: Effects of vertical wind shear on the cumulus transport of momentum: Observations and parameterization. *J. Atmos. Sci.,* **51,** 1640–1660.

——, X.-Z. Liang, and G. J. Zhang, 2003: Seasonal migration of ITCZ precipitation across the equator: Why can't GCMs simulate it? *Geophys. Res. Lett.,* **30,** 1824, doi:10.1029/2003GL017198.

Xie, P., and P. A. Arkin, 1997: Global precipitation: A 17-year monthly analysis based on gauge observations, satellite estimates, and numerical model outputs. *Bull. Amer. Meteor. Soc.,* **78,** 2539–2558.

Zebiak, S. E., 1982: A simple atmospheric model of relevance to El Niño. *J. Atmos. Sci.,* **39,** 2017–2027.

——, and M. A. Cane, 1987: A model El Niño–Southern Oscillation. *Mon. Wea. Rev.,* **115,** 2262–2278.

Zhang, G. J., and H.-R. Cho, 1991a: Parameterization of the vertical transport of momentum by cumulus clouds. Part I: Theory. *J. Atmos. Sci.,* **48,** 1483–1492.

——, and ——, 1991b: Parameterization of the vertical transport of momentum by cumulus clouds. Part II: Application. *J. Atmos. Sci.,* **48,** 2448–2457.

——, and N. A. McFarlane, 1995: Sensitivity of climate simulations to the parameterization of cumulus convection in the CCC-GCM. *Atmos.–Ocean,* **3,** 407–446.

——, and X. Wu, 2003: Convective momentum transport and perturbation pressure field from a cloud-resolving model simulation. *J. Atmos. Sci.,* **60,** 1120–1139.

Zhang, Z., and T. N. Krishnamurti, 1996: A generalization of Gill's heat-induced tropical circulation. *J. Atmos. Sci.,* **53,** 1045–1052.

Zhu, P., and C. S. Bretherton, 2004: A simulation study of shallow moist convection and its impact on the atmospheric boundary layer. *Mon. Wea. Rev.,* **132,** 2391–2409.